ELSEVIER

Chemical Engineering Journal 138 (2008) 341–348

Chemical Engineering Journal

www.elsevier.com/locate/cej

Preparation of nano-alumina trihydroxide by carbonation with surfactants in non-Newtonian fluid

Lei Liang, Fen Guo *, Jianfeng Chen

Research Center of the Ministry of Education for High Gravity Engineering and Technology, Beijing University of Chemical Technology, Beijing 100029, China

Received 14 November 2006; received in revised form 22 May 2007; accepted 1 June 2007

Abstract

The viscosity of the suspension evolved to a viscous non-Newtonian fluid during carbonation precipitation of the nano-alumina trihydroxide (ATH). The high viscosity affected mass transfer and carbonation process evidently. At high viscosity, conventional methods improved mass transfer less than viscosity breaking. Therefore, the surfactants were selected by improving the fluidity of nano-ATH filter cake, among which a polycarboxylate plus CTAB led to a concentrated caustic ATH suspension of 40 wt% content with good fluidity under current experimental conditions, i.e. pH > 12 and $[Na^+] = 2.7\ mol\ L^{-1}$. The surfactants in the carbonation reaction strongly reduced the suspension's viscosity, resulting in the shortening of reaction time and the increment of productivity. TGA and FTIR results demonstrated that the nano-ATH adsorbed 1.2 wt% of the surfactants in dry mass, and that the nano-ATH was hexagon-shaped slice with good dispersion and uniform distribution with a size of ca. 100 nm × 10 nm.

Keywords: Nano-particle; Alumina trihydroxide; Non-Newtonian; Mass transfer; Surfactant; Carbonation

1. Introduction

Having a better flame retardancy and higher filling percentage without distinctly affecting the chemical and physical properties of the matrix, ultrafine or nano-alumina trihydroxide (ATH) is much more preferred and intensively explored as compared with micro-scale ATH [1,2]. Mechanical behaviors of nanocomposites depend strongly on interfacial dispersion and adhesion qualities of nano-scale ATH, whereas nano-scale ATH likely agglomerates in preparation and in polymer matrix. The coupling agent and surface-modified filler are often utilized to solve the agglomeration in polymer while the agglomeration is intractable in the preparation such as Bayer process and carbonation process. Bhattacharya et al. [3] studied the effects of a number of parameters on the precipitation of ATH from actual plant Bayer liquor and observed that ATH particle size could be reduced to less than 1 μm. Chen et al. [1,4] prepared nano-fibers of aluminum hydroxide (AH) and nano-ATH by carbonation in rotating packed bed (RPB).

During Bayer process crystallization ATH particle size enlargement is mainly arisen from particle agglomeration [5,6]. Accordingly, it is important to understand and control the agglomeration process of ATH crystals during their precipitation from Bayer liquors. The agglomeration kinetics of ATH as a function of different experimental parameters including temperature, supersaturation, seed mass, stirring rate and seed size were determined early [7]. Then the agglomeration kinetics was found to be directly controlled by ATH particle interactions in Bayer liquors and was dependent on aluminate supersaturation, temperature and hydrodynamic conditions [5]. However, due to the paucity of understanding concerning ATH particle interactions under the high alkalinity and high salt conditions of the Bayer process, incorporating the particle interaction potential directly with agglomeration models in ATH precipitation has been developing. For thermodynamically unstable systems like concentrated colloidal dispersions, the addition of a dispersant is needed to limit or prevent particle agglomeration [8]. Actually, the surfactants have played crucial roles in preparing nano-structured particles in emulsions [9], microemulsions [10] and microemulsion-assisted precipitation [11]. It was found that they could influence the particle size, morphological properties and the final product requested. Utilization of surfactant is

* Corresponding author. Tel.: +86 10 64413196; fax: +86 10 64434784.
E-mail address: guof@mail.buct.edu.cn (F. Guo).

1385-8947/$ – see front matter © 2007 Elsevier B.V. All rights reserved.
doi:10.1016/j.cej.2007.06.002

Nomenclature

D_L	diffusion coefficient ($m^2\ s^{-1}$)
k_La	volumetric mass transfer coefficient of liquid phase (min^{-1})
R	particle radius (nm)

Greek letters

γ	shear rate (s^{-1})
η	viscosity (mPa s)
φ	volume percentage of the disperse phase (%)

the other possible way to control agglomeration on the basis of experimental parameters studies in Bayer process and carbonation.

High viscosity of non-Newtonian fluid deteriorates the micromixing and mass transfers occurring in many reactors [12] and unit operations including extraction and absorption. Especially in the preparation of nano-powders in liquid phase, the viscosity dramatically enhances because of the huge specific surface area of the product. To obtain nano-particles with narrow size distribution by the reactive precipitation method, a high degree of supersaturation and uniform spatial concentration distribution of the product solute are indispensable, and micromixing is a key factor to meet these requirements [1]. In order to enhance the micromixing, some ways are well discussed and available, such as strengthening stirring, optimizing agitating blade and adopting novel reactors [1]. But the power of agitation cannot increase unboundedly. As the viscosity gains, the effect of raising the Reynolds number diminishes gradually [13]. Thus viscosity breaking is another effective approach to improve micromixing. Surfactant has been used to reduce the viscosity of the suspension and to stabilize the suspension of the nano-powders [14]. Thus surfactant possesses the potential to intensify mass transfer while preventing agglomeration.

2. Experiment

2.1. Materials

The raw material of ATH adopted in this study was an industrial product from Changcheng Aluminum Co. (Zhengzhou, China). Analytical grade sodium hydroxide and food grade CO_2 were used in the experiment. NaOH and ATH (molar ratio about 1.3) were boiled to get the sodium aluminate solution (SA), which was filtrated to obtain a clear liquid. By introducing CO_2 with the clear SA in a four-necked flask, carbonation was performed with agitation at room temperature until pH of the suspension reached about 12 to yield nano-ATH carbonation suspension. Then the suspension discharged from the flask was filtered and rinsed with water for three times to obtain nano-ATH filter cake, followed by drying at 100 °C to obtain nano-ATH powder. Nano-ATH adsorbed surfactants (ATH_2) was obtained by carbonation under conditions similar to the above-mentioned method and surfactants were added when SA turned to turbid.

The aqueous suspensions were prepared by mixing nano-ATH powder with water in high-speed disperser.

2.2. Reagents

Among the reagents tested, anionic dispersers were commercially available polymer surfactants and others were analytically pure samples.

The selected surfactants were added dropwise to about 5 g of the nano-ATH filer cake and then a scoop was used to mix them. If the reagent was active, the cake turned into suspensions. Afterwards, a few drops of saturated Na_2CO_3 solution and NaCl solution (19 wt%) were added to the suspensions. Those surfactants that reduced the viscosity of the suspension in the initial stage were mostly inactive under the caustic conditions, among which a polycarboxylate (25 wt% solution, Orotan 731A, Rohm and Haas, USA) plus CTAB (cetyltrimethyl ammonium bromide solution, 7.3 wt%) kept their properties.

2.3. Morphology and size analysis

Particle morphology and size analysis were performed by a H-800 Electron Microscope (HITACHI, Japan). The powder of nano-ATH and -ATH_2 were dispersed in deionized water and the time of ultra sonic dispersion was about 5 min.

2.4. Viscosity measurements

The viscosity was measured by the bi-directional Brookfield DV-111+ Rheometer. Recorded automatically via a built-in program, a plot of viscosity versus shear rate was made as the shear rate was increased to a certain value, then immediately decreased to the starting point. Note that the "up" and "down" curves do not coincide. This "hysteresis loop" is the criterion of rheopexy and thixotropy. A Brookfield TC-101 temperature bath was used to keep the temperature at 20 °C and solid contents of nano-ATH suspensions were 9.4 wt% if not mentioned explicitly.

2.5. FTIR spectroscopy

Infrared measurements were made on a Nicolet-210 FTIR (USA). ATH and ATH_2 powder mixed with KBr and pressed into pellets before recording the spectra. The OH-stretching frequencies of well-crystallized gibbsite are at 3623, 3527, 3460, 3396 and 3384 cm^{-1}. Bayerite shows four OH-stretching bands at 3653, 3550, 3463 and 3435 cm^{-1} [15]. The absorption peaks in Fig. 1(a) at 3656, 3621, 3550, 3527 and 3476 cm^{-1} prove that the nano-ATH and -ATH_2 were well-crystallized blend of gibbsite and bayerite. Intensity of the distinctive peaks of ATH_2 descended slightly; these results demonstrated some changes of surface chemistry of ATH_2 particles by the addition of surfactants. The absorption peaks at the 1560 and 1700 cm^{-1} attribute to CO_2^- asymmetrical stretching of carboxylate and CO^- stretching vibration of carboxylic acid, respectively. The bands at 1100–1300 cm^{-1} are due to the typical signals of C–N and bands at 1475 and 1400 cm^{-1} are the characteristic absorp-

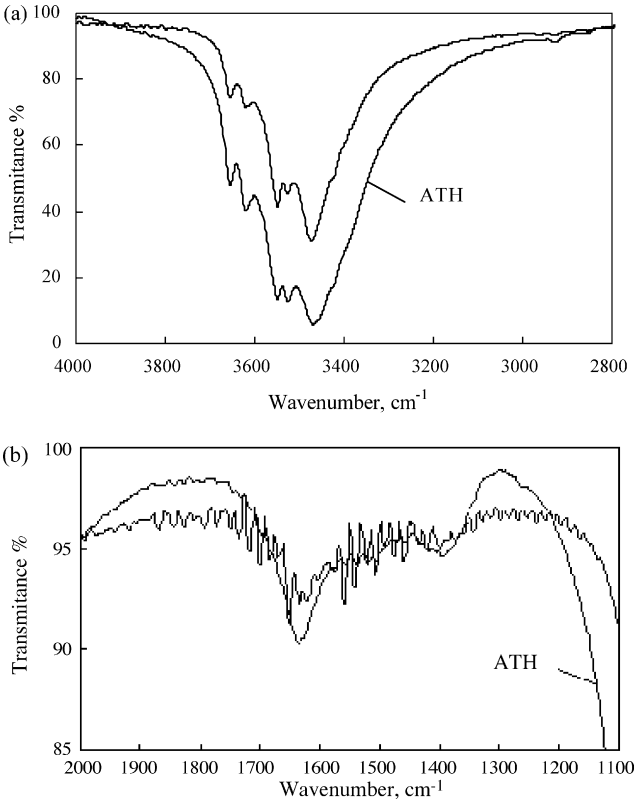

Fig. 1. FTIR graphs of nano-ATH and nano-ATH_2: (a) band form 4000 to 2800 cm^{-1} and (b) band form 2000 to 1100 cm^{-1}.

tion peaks of CTAB. FTIR results showed that both surfactants were adsorbed on the nano-ATH_2.

2.6. Adsorption measurements

In order to determine the amount of surfactants adsorbed, ATH filter cake was analyzed by thermal gravimetric analysis (TGA) (Model STA 499C, Netzsch Inc., Germany) at a heating rate of 10 °C min^{-1} in an N_2 atmosphere. The TGA data showed a three-step pyrolysis, i.e. the removal of absorbed water (20–120 °C), the transformation of ATH to Al_2O_3 (120–350 °C), and the decomposition of surfactant (350–600 °C) [15]. Water content of the nano-ATH filter cake ranges 66–70 wt%, indicating that the volume of nano-ATH powder surrounded with water is more than 4.8 times than itself (density of ATH is about 2.43 g cm^{-3}) and the maximal solid content of nano-ATH suspension without surfactants is about 33.3 wt%.

Fig. 2 showed that the amount of absorbed water of ATH_2 cake was 42%, much lower than the 66–70% of the nano-ATH cakes because the surfactant releases some absorbed water. As a result, the cake incorporating the surfactant can flow and then the vacuum pump can suction more water from cake. The weight loss of dry ATH is 34.64% in theory and is around 34% in this experiment owing to the existence of residual hydroxyl even after 900 °C. The nano-ATH_2 weight loss from 120 to 600 °C is 35.18%, which indicates the existence of adsorbed surfactant. Considering the ATH still losses weight even after 350–600 °C, the data of surfactant loss was obtained by subtracting the corresponding data of a control ATH (loss 33.97% from 120 to 600 °C). The result shows the adsorbed surfactant is 1.2 wt% in dry mass (4.8 wt% in wet mass and the amount of CTAB is neglected in calculation) of ATH_2. The adsorbed mass is higher even than the dosage of surfactants under mild condition due to coiled configuration adsorption at alkaline region [16].

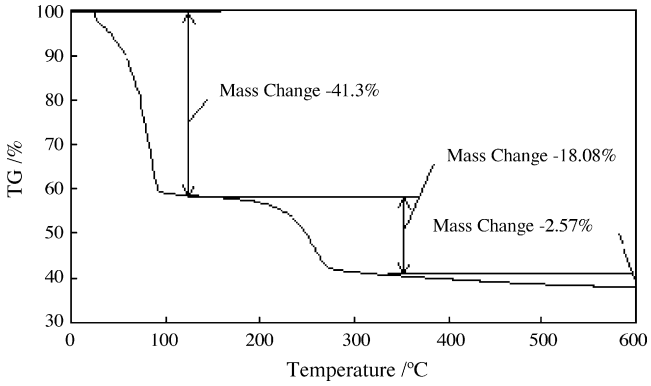

Fig. 2. TGA graph of nano-ATH_2.

2.7. BET surface area

BET surface area was determined by ASAP 2010 Analyzer (Micromeritics, USA) to evidence the particle size and to elucidate the improved dispersibility of nano-ATH particle by surfactants.

2.8. XRD

Particle crystal structure analysis was conducted with a HZG4 Multicrystal Diffractometer (Carl Zeiss Jane Company, Germany), radiation Cu Kα 40 kV = 25 mA and scanning speed at 2 °/min. XRD pattern of the product ATH_2 is shown in Fig. 3, which is in good agreement with the characteristic spectrum of bayerite crystal in the JCPDS database.

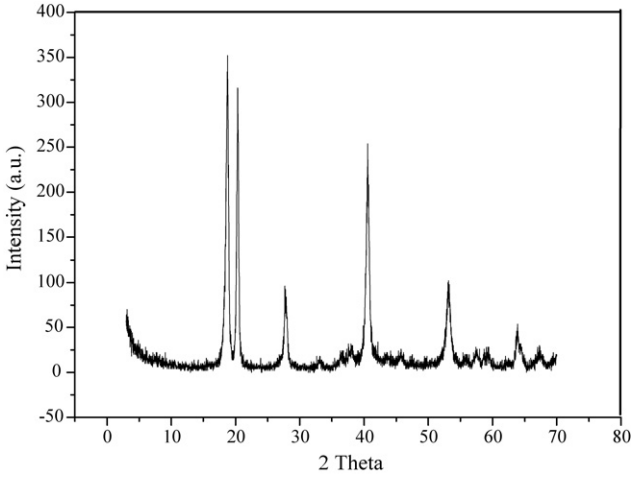

Fig. 3. XRD pattern of ATH_2.

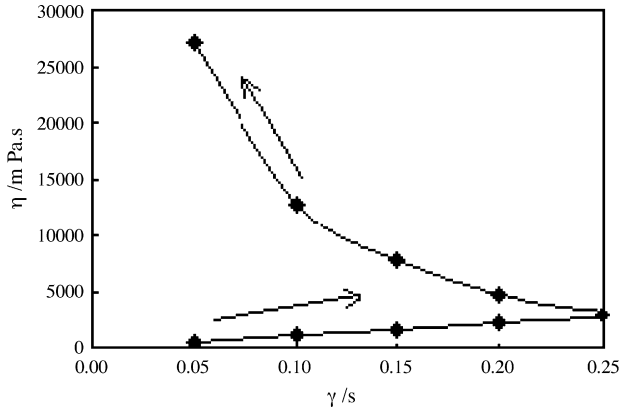

Fig. 4. UPDOWN flow curve of ATH suspension by carbonation at shear rate from 0.05 to 0.25 s^{-1}.

3. Results and discussion

3.1. Viscous suspension from carbonation and carbonation dominated by high viscosity

Figs. 4 and 5 illustrate the ATH suspension from carbonation acts as a dilatant and pseudo-plastic non-Newtonian fluid at low and high shear rate, respectively; it is also a time-dependent fluid with obvious rheopexy at low shear rate and a little thixotropy at high shear rate. The viscosity decreases gradually after 30 s^{-1} and reaches 360 mPa s at 50 s^{-1}. The nano-ATH network is the origin of the high viscosity and complex fluid behavior [17]. At low shear rates, the aggregates may be deformed but remain almost intact (dilatant). As the shear rate is increased, the aggregates may be broken down into individual flocs, resulting to the decrease of viscosity with decreasing friction (pseudoplastic).

The following formula, given by Wierenga et al. [18], gives a qualitative relationship for dilute suspensions, without considering the particle bonding force:

$$\eta_r = \eta_0 \left(1 + a\varphi + \frac{b\Delta R\varphi}{R} + c\varphi^2\right) \quad (1)$$

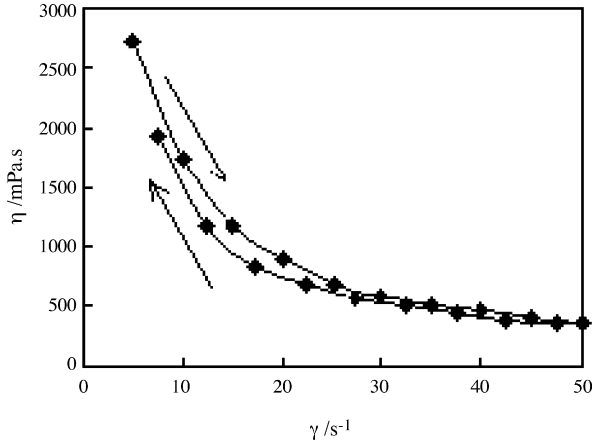

Fig. 5. UPDOWN flow curve of ATH suspension by carbonation at shear rate from 5 to 50 s^{-1}.

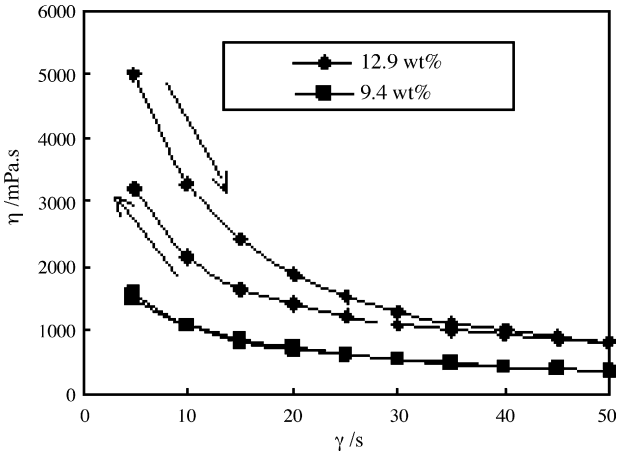

Fig. 6. UPDOWN flow curves of aqueous ATH suspensions at different solid contents.

where η_0 is the viscosity of the continuous phase, φ the volume percentage (V%) of the disperse phase, ΔR the thickness of adsorption layer and R is the particle radius. The equation reveals that volume percentage plays an important role in viscosity because it appears in each term. As displayed in Fig. 6, the viscosity of aqueous suspensions increases from 355 to 820 mPa s at 50 s^{-1} when solid content varies from 9.4 to 12.9 wt%. Furthermore, as the particle size diminishes, the $\Delta R/R$ will increase fast. The bigger the specific surface area is, the more water the particle adsorbs. As a result, the volume of the particle becomes bigger, and in the end the viscosity of their suspensions will tend to be high.

For the instantaneous or viscous reaction system, the reaction rate becomes micromixing-dependent. It was found that the mixing became poor with an increase in viscosity to different extent depending on viscosity ranges, and that improving mixing by intensifying agitation was available only within a range of rotational speed, and that the critical operating speed was related to fluid pseudoplastic property. Carbonation includes an instantaneous precipitation reaction and a comparatively slow reaction that CO_2 neutralizes hydroxyl in the solution. The latter determines the rate of SA carbonation [1].

As the carbonation goes on, the non-Newtonian property brings complex problems to mixing and mass transfer. The diffusion coefficient (D_L) and volumetric mass transfer coefficient of liquid phase (k_La) will reduce. The effect of viscosity is generally expressed as $k_La \propto \eta^n$, and for the non-Newtonian system, the n ranges from −0.25 to −1.01 [19,20], which means that the k_La at the end of the reaction is much smaller than the k_La at the start. Thus reaction rate of carbonation is dominated by mass transfer of CO_2 through the liquid film for reaction under the pure CO_2 atmosphere. The reaction will stagnate when suspension viscosity reaches a point about 300 mPa s. In other words, solid content of ATH will not develop unless its size gets bigger because viscosity is the function of solid content and particle radius. As illustrated in Table 1, the contents of final nano-ATH suspension without surfactants at different SA concentrations are all nearly 80 g L^{-1}, which causes the productivity declines as the SA concentration rises. It should be noted that when the

Table 1
Carbonation process conditions and related results

No.	[SA] (mol L^{-1})	Surfactants	Gas flow rate (L/min)	Reaction time (min)	Productivity
1	2	No	0.2	17	0.48
2	2	Yes	0.2	9	0.8
3	4	No	0.2	22	0.25
4	4	Yes	0.2	17	0.66
5	1	No	0.1	14	0.6

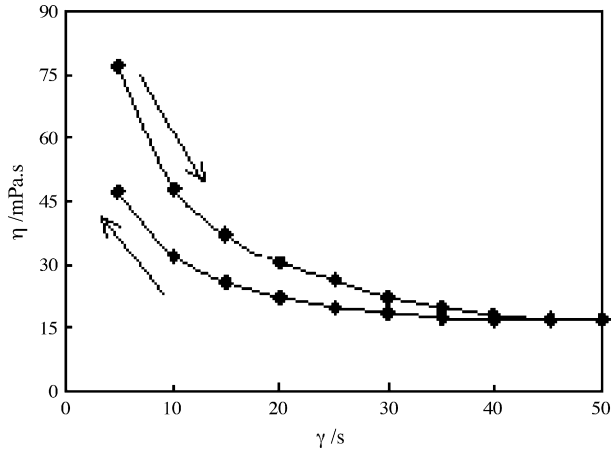

Fig. 7. UPDOWN flow curves of nano-caustic ATH suspensions with surfactants at pH > 12 and $[Na^+] = 2.7\ mol\ L^{-1}$, polycarboxylate 15 wt% of ATH, CTAB 3.5 wt% of ATH.

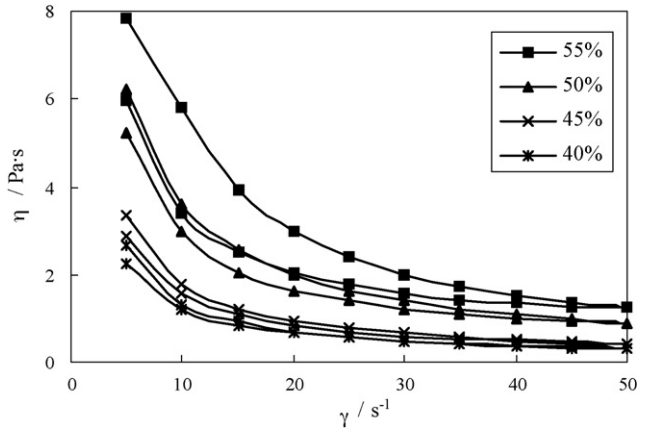

Fig. 8. UPDOWN flow curves of the concentrated caustic ATH suspensions with surfactants at pH > 12 and $[Na^+] = 2.7\ mol\ L^{-1}$.

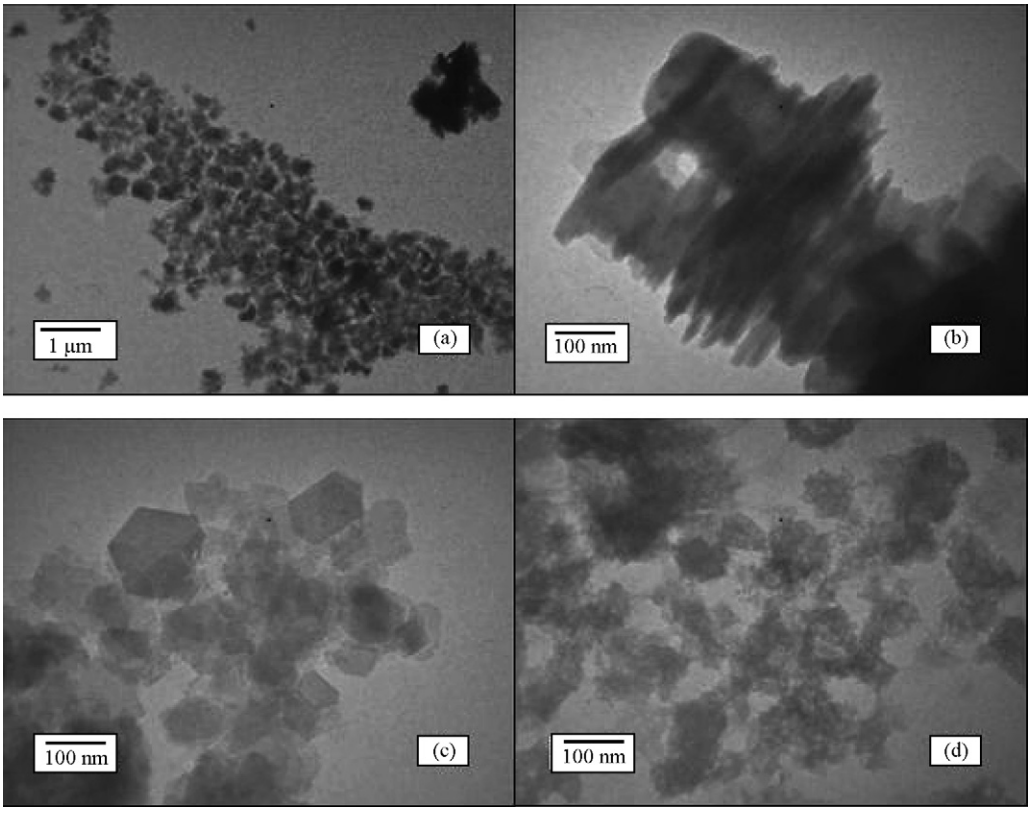

Fig. 9. TEM images of the nano-ATH by the carbonation $[SA] = 2\ mol\ L^{-1}$: (a) 10k×; (b) 100k×; (c) the time of ultra sonic dispersion is 30 min, 100k×; (d) ATH surrounded with AH, 100k×.

cementation happens, the particle size will reach micron grade. Further, the solid content affects the viscosity very little and productivity can reach 90% at different SA concentrations.

3.2. Mass transfer intensified by surfactants

Surfactants or active substances were utilized to intensify the mass transfer in some process with the most emphasis on their functions to interface [21]. In theory, surfactants that diminish the viscosity can also intensify the mass transfer in viscous suspension. The flow curve of the caustic suspension added with the mentioned surfactants is displayed in Fig. 7, in which the fluid keeps non-Newtonian. This indicates that some bonding of hydroxyl groups maintains even in high ion concentration system. However, viscosity at shear rate 50 s^{-1} is an order of magnitude lower than its origin.

The surfactants were used to prepare a series of concentrated caustic suspensions. Compared to the significant enhancement of viscosity as solid content changes (Fig. 6), the viscosity rises smoothly as shown in Fig. 8 because the different mechanism at high concentrations [22]. The obtained caustic suspension of 40 wt% had similar flow curve as carbonation suspension of 9.4 wt% and its viscosity at shear rate 50 s^{-1} is 317 mPa s versus 360 mPa s of its counterpart. The excellent liquidity of the diluent suspensions and the fluidity of the concentrated suspensions with surfactants all hint that, with same agitation, the carbonation with surfactants can reach higher productivity in a shorter time than the carbonation without surfactants do.

The carbonation without and with mentioned surfactants were processed under similar conditions. In Table 1 the productivity is highly enhanced with surfactants, because they reduce the viscosity a lot and suspension can hold more particles at the same viscosity level. The productivity with surfactants still decreases by increasing the SA concentration because the viscosity also rises along with the increase of the solid content in suspension with surfactants. Also the reaction time of carbonation with surfactants is shortened, which allows reaching high productivity at equal [SA], as shown in Table 1. The solid content strongly affects the gas–liquid mass transfer and reaction in slurry system [23]. In the range of low solid content (<4%), enhancement of mass transfer may be realized. When the solid content is above 1%, the effect of particle on viscosity must be taken into account [24]. For ATH carbonation, solid content soon surpasses the range that viscosity can be neglected. So the mass transfer in carbonation is intensified radically by surfactants that decreased the viscosity.

3.3. Agglomeration restrained by surfactants in carbonation

Fig. 9a and b illustrates that the powders from carbonation without surfactants are poorly dispersed macroscopically and microscopically, and the size of the secondary particle is around 500 nm. In Fig. 9(b), a dozen of slices tightly overlap vertically or horizontally. After 30 min of ultra sonic dispersion, particles in Fig. 9(c) are separated and appear to be hexagon-shaped slice. This suggests that the ATH particles do not cement severely, and reversible aggregation is the main cause of the poor dispersion. From the figure one can see that the primal particle size is about 200 nm × 20 nm ($L \times T$). Some nano-fibers of AH, which appear only after the pH value is under 11 in carbonation usually [1], emerge on the surface of ATH particles (see Fig. 9(d)). This manifests that high viscosity induces the segregation in system, slow dispersion of CO_2 into liquid phase and the accumulation of CO_2 in some regions.

TEM images of the ATH powder from carbonation with surfactants are depicted in Fig. 10, which contrasts sharply with those without surfactants under same process conditions. Fig. 10(a) shows that ATH powder disperses well macroscopi-

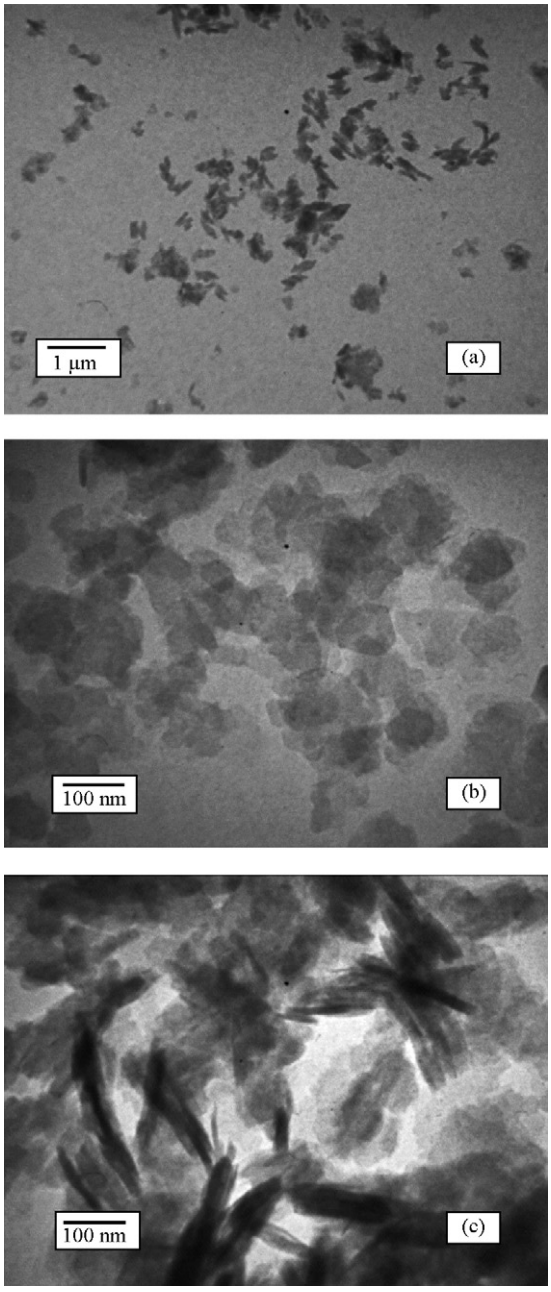

Fig. 10. TEM images of the nano-ATH_2 by the carbonation with surfactants: (a) 10k×, [SA] = 4 mol L^{-1}; (b) 100k×, [SA] = 2 mol L^{-1}; (c) 100k×, [SA] = 4 mol L^{-1}.

cally and the secondary particle size is about 0.25 μm. According to Fig. 10(b) and (c), particle is hexagon-shaped slice and the primal particle size is 100 nm × 10 nm ($L \times T$). Several slices stack loosely and separate well microscopically. The horizontally overlapped layers are rather thin that they appear to be transparent. Organic compounds cause changes in ATH morphologies in SA. At higher mannitol concentrations, thinner crystalline plates are formed, indicative of inhibition on the basal face relative to the prismatic faces [25]. Polycarboxylate with more hydroxyls causes the increase of organic adsorption on the ATH surface, and hence thinner plate is obtained.

It is known that excellent dispersibility is critical for nanomaterials' application. BET surface area of nano-ATH carbonated with surfactants is 82 m^2/g compared with the 30 m^2/g by RPB [4]. Since the particle size changes limitedly, it is the improved dispersion of nano-particles more than the diminished particle size that can mostly account for the much higher surface area. The improvement of particle size and dispersibility comes from the steric hindrance of the surfactants that adsorb on the particle surface, which prevents particles from aggregation and bonding. Therefore, the secondary particle formation is difficult, which restrains the particle size growth via cementation. High viscosity may inhibit crystal growth and cementation, so the suspension with high supersaturation can be stable for a period of time. But when the suspension is filtered or rinsed, cementation and agglomeration can be easily produced and secondary particles become bigger and more rigid, which brings poor dispersibility. While the productivity improved by surfactants and the supersaturation-to-particle surface area ratio reduced, the trend of aggregation and cementation is small. In this case, an even particle size and good dispersability were achieved.

4. Conclusions

The particles size of alumina trihydroxide obtained from the carbonation precipitation is 200 nm × 20 nm ($L \times T$). The powder is poorly dispersed macroscopically and microscopically with the size of the secondary particle around 500 nm, and reversible aggregation is the cause of the poor dispersion. The rheology showed that the suspension was the dilatant and the pseudo-plastic non-Newtonian fluid at the low and high shear rate, respectively. It is also a time-dependent fluid with obvious rheopexy at low shear rate and a little thixotropy at high shear rate.

Surfactants were selected by improving fluidity of nano-ATH filter cake and a polycarboxylate plus CTAB kept their properties and leaded to a concentrated ATH suspension of 40 wt% content in a solution of pH above 12 and $[Na^+] = 2.7\ mol\ L^{-1}$.

The viscosity of the suspension during the carbonation precipitation of the ATH increases along with the solid content rising and particle size diminishing. The high viscosity of non-Newtonian fluid deteriorates the mass transfer and reaction process. The carbonation rate depends on mass transfer rate through the liquid film, which is dominated by the viscosity and stagnates when the solid content of nano-ATH is above 8 wt%. As a result, the productivity of the reaction is low and the aluminum hydroxide emerges. The surfactants were utilized in the carbonation reaction, and the process was investigated, and the characteristics of the nano-ATH were analyzed. The surfactants strongly reduced the viscosity of the suspension, so the mass transfer was intensified, reaction time was shortened, productivity increased and the water content of the ATH filter cake fallen. Finally, the nano-ATH_2 was even and well dispersible hexagon-shaped slice with size about 100 nm × 10 nm. The DTA and FTIR showed that the nano-ATH_2 adsorbed 1.2 wt% of the surfactants in dry mass, which brought the reaction excellent particle dispersibility and even particle size. Agglomeration restrained and mass transfer intensified was achieved in non-Newtonian carbonation process by surfactants by means of steric hindrance and viscosity reduction.

Acknowledgement

This work was supported by the National '863' program of China (2002AA302605).

References

[1] J.F. Chen, L. Shao, F. Guo, X.M. Wang, Synthesis of nano-fibers of aluminum hydroxide in novel rotating packed bed reactor, Chem. Eng. Sci. 58 (2003) 569–575.
[2] X.G. Zhang, F. Guo, J.F. Chen, G.Q. Wang, H. Liu, Investigation of interfacial modification for flame retardant ethylene vinyl acetate copolymer/alumina trihydrate nanocomposites, Polym. Degrad. Stab. 87 (2005) 411–418.
[3] I.N. Bhattacharya, J.K. Pradhan, P.K. Gochhayat, S.C. Das, Factors controlling precipitation of finer size alumina trihydrate, Int. J. Miner. Process. 65 (2002) 109–124.
[4] D.G. Wang, F. Guo, J.F. Chen, H. Liu, Z.T. Zhang, Preparation of nano-aluminium trihydroxide by high gravity reactive precipitation, Chem. Eng. J. 121 (2006) 109–114.
[5] C.A. Prestidge, I. Ametov, Cation effects during aggregation and agglomeration of gibbsite particles under synthetic Bayer crystallisation conditions, J. Cryst. Growth 10 (2000) 924–933.
[6] I. Seyssiecq, S. Veesler, R. Boistelle, A non-immersed induction conductivity system for controlling supersaturation in corrosive media: the case of gibbsite crystals agglomeration in Bayer liquors, J. Cryst. Growth 169 (1996) 124–128.
[7] I. Seyssiecq, S. Veesler, R. Boistelle, J.M. Lamerant, Agglomeration of Gibbsite $Al(OH)_3$ crystals in Bayer liquors. Influence of the process parameters, Chem. Eng. Sci. 53 (1998) 2177–2185.
[8] H. Bouhameda, S. Boufia, A. Magninb, Alumina interaction with AMPS-PEG random copolymer. II. Stability and rheological behavior, Colloid Surf. A 253 (2005) 145–153.
[9] A. Martínez, C. González, M. Porras, J.M. Gutiérrez, Nano-sized latex particles obtained by emulsion polymerization using an amphiphilic block copolymer as surfactant, Colloid Surf. A 270 (2005) 67–71.
[10] M. Porras, A. Martínez, C. Solans, C. González, J.M. Gutiérrez, Ceramic particles obtained using W/O nano-emulsions as reaction media, Colloid Surf. A 270 (2005) 189–194.
[11] V. Uskoković, M. Drofenik, A mechanism for the formation of nanostructured NiZn ferrites via a microemulsion-assisted precipitation method, Colloid Surf. A 266 (2005) 168–174.
[12] A. Elgozali, V. Linek, M. Fialová, O. Wein, J. Zahradník, Influence of viscosity and surface tension on performance of gas–liquid contactors with ejector type gas distributor, Chem. Eng. Sci. 57 (2002) 2987–2994.
[13] J. Min, Experimental studs and numerical simulation of macromixing & micromixing in stirred tank, Ph.D. dissertation, Beijing University of Chemical Technology, China 2005.
[14] L.P. Zhao, L. Gao, Fabrication and surface characterization of NH_4PAA-stabilized HAZ suspensions, J. Colloid Interf. Sci. 262 (2003) 428–434.

[15] M.P. Albano, L.B. Garrido, A.B. Garcia, Dispersion of aluminum hydroxide coated Si_3N_4 powders with ammonium polyacrylate dispersant, Colloid Surf. A 181 (2001) 69–78.
[16] Y.Q. Liu, L. Gao, J.k. Guo, Adsorption of acrylic copolymers at the alumina–water interface, Colloid Surf. A 174 (2000) 349–356.
[17] F. Yziquel, P.J. Carreau, M. Moan, P.A. Tanguy, Rheological modeling of concentrated colloidal suspensions, J. Non-Newtonian Fluid Mech. 86 (1999) 133–155.
[18] A.M. Wierenga, T.A.J. Lenstra, A.P. Philipse, Aqueous dispersions of colloidal gibbsite platelets: synthesis, characterisation and intrinsic viscosity measurements, Colloid Surf. A 134 (1998) 359–371.
[19] F. Garcia-Ochoa, E. Gomez, Theoretical prediction of gas–liquid mass transfer coefficient, specific area and hold-up in sparged stirred tanks, Chem. Eng. Sci. 59 (2004) 2489–2501.
[20] V. Linek, M. Kordac, T. Moucha, Mechanism of mass transfer from bubbles in dispersions. Part II. Mass transfer coefficients in stirred gas–liquid reactor and bubble column, Chem. Eng. Process. 44 (2005) 121–130.
[21] J. Zahradnik, G. Kuncova, M. Fialova, The effect of surface-active additives on bubble coalescence and gas holdup in viscous aerated batches, Chem. Eng. Sci. 54 (13) (1999) 2401–2408.
[22] R. Lapasin, M. Grassi, S. Pricl, Rheological modeling of fractal and dense suspensions, Chem. Eng. J. 64 (1996) 99–106.
[23] A.A. Barresi, Selectivity of mixing-sensitive reactions in slurry systems, Chem. Eng. Sci. 55 (2000) 1929–1933.
[24] C. Freitas, J.A. Teixeira, Oxygen mass transfer in a high solids loading three-phase internal-loop airlift reactor, Chem. Eng. J. 84 (2001) 57–61.
[25] W.V. Bronswijk, H.R. Watling, Z. Yu, A study of the adsorption of acyclic polyols on hydrated alumina, Colloid Surf. A 157 (1999) 85–99.